PROCEEDINGS OF THE ROYAL SOCIETY A

Proc. R. Soc. A (2012) **468**, 1041–1064
doi:10.1098/rspa.2011.0476
Published online 7 December 2011

The thickness of the falling film of liquid around a Taylor bubble

By E. W. Llewellin[1,*], E. Del Bello[2], J. Taddeucci[2], P. Scarlato[2] and S. J. Lane[3]

[1]*Department of Earth Sciences, Durham University, South Road, Durham DH1 3LE, UK*
[2]*Department of Seismology and Tectonophysics, Istituto Nazionale di Geofisica e Vulcanologia, Via di Vigna Murata 605, 00143 Rome, Italy*
[3]*Lancaster Environment Centre, Lancaster University, Lancaster LA1 4YQ, UK*

We present the results of laboratory experiments that quantify the physical controls on the thickness of the falling film of liquid around a Taylor bubble, when liquid–gas interfacial tension can be neglected. We find that the dimensionless film thickness λ' (the ratio of the film thickness to the pipe radius) is a function only of the dimensionless parameter $N_f = \rho\sqrt{gD^3}/\mu$, where ρ is the liquid density, g the gravitational acceleration, D the pipe diameter and μ the dynamic viscosity of the liquid. For $N_f \lesssim 10$, the dimensionless film thickness is independent of N_f with value $\lambda' \approx 0.33$; in the interval $10 \lesssim N_f \lesssim 10^4$, λ' decreases with increasing N_f; for $N_f \gtrsim 10^4$ film thickness is, again, independent of N_f with value $\lambda' \approx 0.08$. We synthesize existing models for films falling down a plane surface and around a Taylor bubble, and develop a theoretical model for film thickness that encompasses the viscous, inertial and turbulent regimes. Based on our data, we also propose a single empirical correlation for $\lambda'(N_f)$, which is valid in the range $10^{-1} < N_f < 10^5$. Finally, we consider the thickness of the falling film when interfacial tension cannot be neglected, and find that film thickness decreases as interfacial tension becomes more important.

Keywords: gas slug; slug flow; long bubble; turbulent falling film; pipe flow; transitional flow

1. Introduction

Taylor bubbles, also called 'gas slugs' and 'long bubbles', are bubbles that almost fill the cross section of a pipe such that their buoyant ascent causes a film of liquid to fall around them, down the walls of the pipe (figure 1). The morphology of Taylor bubbles has been described in detail by previous workers (e.g. Goldsmith & Mason 1962; Campos & Guedes de Carvalho 1988; Bugg *et al.* 1998, Viana *et al.* 2003, Feng 2008) and is summarized in figure 1. The bubble can be divided into four regions: (1) an approximately hemispherical, or prolate-hemispheroidal nose,

*Author for correspondence (ed.llewellin@durham.ac.uk).

Received 4 August 2011
Accepted 7 November 2011

This journal is © 2011 The Royal Society

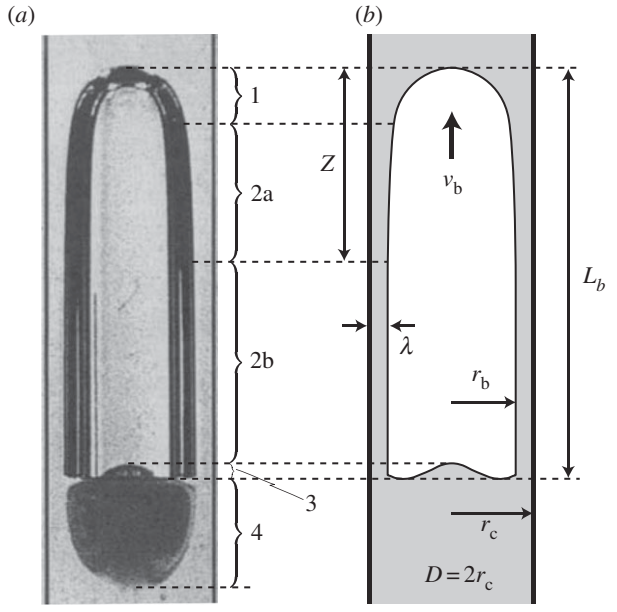

Figure 1. (*a*) An image (reproduced with permission from Campos & Guedes de Carvalho (1988), copyright © Cambridge University Press) and (*b*) interpretative diagram of a Taylor bubble of air, of length $L_b = 0.051$ m, ascending a cylindrical pipe of internal diameter $D = 0.019$ m, filled with an aqueous solution of glycerol ($N_f = 437$; see §2*a* for definition). The bubble can be divided into four distinct regions: (1) nose, (2) body, (3) tail, and (4) wake. Around the lower part of the body region (2b), the film has achieved its equilibrium thickness λ. In this example, the wake appears dark because it contains a dyed liquid (see Campos & Guedes de Carvalho 1988, for details).

(2) a body region surrounded by a falling liquid film, (3) a tail region of variable morphology, which may be hemispheroidal, flat or concave, and (4) a wake, which may be open and laminar, closed (i.e. with recirculating vortices, as shown in figure 1) or turbulent. The body region can be subdivided: around the upper part (2a), the developing film is accelerating and thinning; around the lower part (2b), the forces acting on the film are in equilibrium and the film has constant thickness λ. We note that it is conventional to use δ for the thickness of a falling film; this practice stems from the assumption, made in most previous studies, that the film is thin. We do not make this assumption, hence our break with convention.

Much of the previous research into the behaviour of Taylor bubbles has been motivated by their importance in industrial and engineering settings, particularly as components of two-phase 'slug flow' (Nicklin *et al.* 1962, Fabré & Liné 1992). This work has included theoretical studies (Dumitrescu 1943; Davies & Taylor 1950; Goldsmith & Mason 1962; Brown 1965; Batchelor 1967), experimental studies (Davies & Taylor 1950; Goldsmith & Mason 1962; White & Beardmore 1962; Campos & Guedes de Carvalho 1988; Viana *et al.* 2003; Nogueira *et al.* 2006) and numerical studies (Taha & Cui 2006; Zheng *et al.* 2007; Feng 2008; Kang *et al.* 2010). A major goal of previous work has been to quantify the physical controls on the ascent velocity v_b of Taylor bubbles (recently reviewed by Viana *et al.* 2003) and the nature of the velocity field in the liquid around them (e.g. Bugg & Saad 2002; Nogueira *et al.* 2006). There is also a large body of previous

work (summarized in Karapantsios *et al.* 1989; Lel *et al.* 2005; Zhou *et al.* 2009) that describes the behaviour of falling liquid films in general (i.e. not specifically associated with the rise of Taylor bubbles).

The present study is motivated by the volcanological importance of Taylor bubbles. Gas slugs (as they are usually called in the volcanology literature) are believed to cause strombolian activity (Blackburn *et al.* 1976). The behaviour of the slugs during ascent influences the nature of the eruptions they cause (Seyfried & Freundt 2000; James *et al.* 2009) and the associated geophysical signals (Vergniolle & Brandesis 1996; Chouet *et al.* 2003, 2010, James *et al.* 2006). In particular, the thickness of the falling magma film influences the development of overpressure during a slug's ascent, and plays a key role in determining eruption explosivity (Del Bello *et al.* accepted). While several theoretical models exist for the thickness of the falling film around a rising Taylor bubble (summarized in §2*b*), there has been no systematic experimental validation of these models over the wide range of dimensionless parameters appropriate for volcanic Taylor bubbles—that is the primary goal of this work.

This study is restricted to Taylor bubbles rising through Newtonian liquids in vertical, cylindrical pipes. The effect of variations in liquid rheology and pipe inclination and cross-sectional shape were considered by, for example, Shosho & Ryan (2001), Taha & Cui (2006) and Amaya-Bower & Lee (2011). We also focus primarily on situations where interfacial tension between the gas and liquid phases is negligible; however, in §5*d*, we consider the implications of relaxing this assumption.

2. Theoretical framework

(*a*) *Characterizing Taylor bubbles*

Much previous work has focussed on the ascent velocity v_b of a Taylor bubble (see Viana *et al.* 2003 for a recent review of experimental data, and Funada *et al.* 2005 for a theoretical perspective). The ascent velocity has been shown to depend on the dynamic viscosity of the liquid μ, its density ρ, the liquid–gas interfacial tension σ, the internal diameter of the pipe D and the gravitational acceleration g. These quantities can be combined to form various dimensionless groups, including (White & Beardmore 1962; Wallis 1969; Seyfried & Freundt 2000)

$$Fr = \frac{v_b}{\sqrt{gD}}, \tag{2.1}$$

$$Mo = \frac{g\mu^4}{\rho\sigma^3} \tag{2.2}$$

and

$$Eo = \frac{\rho g D^2}{\sigma}. \tag{2.3}$$

These are, respectively, the Froude number—which is a dimensionless velocity, representing the ratio of inertial and gravitational forces; the Morton number—which represents the ratio of viscous and interfacial tension forces; and the Eötvös number—which represents the ratio of buoyancy and interfacial tension forces. Interfacial tension plays a negligible role in determining the behaviour of a Taylor

bubble when $Eo > 40$ (Viana *et al.* 2003), in which case, the morphology and ascent velocity of the bubble are controlled by inertial and viscous forces. These conditions are met for all volcanic slugs (Seyfried & Freundt 2000), as well as for many situations of industrial and engineering importance. The Morton and Eötvös numbers can be combined to eliminate interfacial tension, yielding a fourth quantity, the 'dimensionless inverse viscosity' (Wallis 1969)

$$N_\mathrm{f} = \left[\frac{Eo^3}{Mo}\right]^{1/4} = \frac{\rho}{\mu}\sqrt{gD^3}, \tag{2.4}$$

which is sometimes presented as the buoyancy Reynolds number (e.g. Viana *et al.* 2003) or Archimedes number ($Ar = N_\mathrm{f}^2$; Kang *et al.* 2010).

An analytical solution for the ascent velocity of a Taylor bubble through an inviscid liquid was found by Dumitrescu (1943), under the assumption—consistent with experimental observations—that the bubble's nose is hemispherical, and that flow in the liquid film is laminar. In this case, which represents inertial control, Dumitrescu found that the Froude number was constant: $Fr = 0.351$. Subsequent experimental work by White & Beardmore (1962) validated this result in the inertial limit but demonstrated that, more generally, the Froude number is a function of N_f and Eo. Since then, many experimental and theoretical studies have sought to quantify $Fr(N_\mathrm{f}, Eo)$. Viana *et al.* (2003) provide a thorough review of this work and synthesize experimental data to produce an empirical 'universal correlation' for Fr. This correlation is rather cumbersome, relying on repeated application of a logistic dose curve. However, Viana *et al.* note that Fr is largely independent of Eo for $Eo > 40$, which holds for the current study, allowing us to simplify the correlation considerably to give

$$Fr = 0.34\left[1 + \left(\frac{31.08}{N_\mathrm{f}}\right)^{1.45}\right]^{-0.71}; \tag{2.5}$$

hence, for the situation of interest (negligible interfacial tension), Froude number is a function of inverse viscosity only. The data synthesized by Viana *et al.* (2003) for $Eo > 40$, cover the inverse viscosity range $10^{-1} < N_\mathrm{f} < 10^5$, so equation (2.5) has a very broad validity; we recommend this equation for calculating the ascent velocity of a Taylor bubble when interfacial tension can be ignored.

A further dimensionless quantity that is employed by some workers to describe Taylor bubbles is the bubble (or slug) Reynolds number (e.g. Nogueira *et al.* 2006; Feng 2008)

$$Re_\mathrm{b} = \frac{\rho v_\mathrm{b} D}{\mu}, \tag{2.6}$$

which represents the ratio of inertial and viscous forces in the liquid. The bubble Reynolds number can be written as the product of the inverse viscosity and the Froude number,

$$Re_\mathrm{b} = N_\mathrm{f}\, Fr; \tag{2.7}$$

hence, from equation (2.5), we can see that the Reynolds number is a function of inverse viscosity only.

(*b*) *Falling liquid films*

Previous work on falling films is not restricted to films around Taylor bubbles; indeed, the largest part of the literature deals with thin liquid films falling down surfaces where Taylor bubbles are not involved. When the film around a Taylor bubble is thin, the local curvature of the pipe can be neglected, and the film behaviour is the same whether it flows down the inside or the outside of a pipe, or down a plane surface (Karapantsios *et al.* 1989). This thin-film assumption is valid in many chemical engineering situations, which typically involve the ascent of Taylor bubbles in pipes that are of the order of centimetres or decimetres in diameter, and which are filled with water or another low-viscosity liquid. In such settings, where N_f and Re_b are large, the falling film around the rising Taylor bubble is thin when compared with the pipe radius (Goldsmith & Mason 1962; Brown 1965; Batchelor 1967); consequently, the extensive literature that deals with thin films is relevant to the current study. In this section, we summarize previous studies that present models for the thickness of thin falling films in general, and of falling films around Taylor bubbles in particular.

Thin falling films are usually characterized, in the chemical engineering literature, by the film Reynolds number Re_f, which is often defined in terms of Γ, the mass flux of liquid per unit breadth of the flow ($\Gamma = \rho\lambda v_\mathrm{f}$, where v_f is the average velocity in the film). The film Reynolds number is given by (Dukler & Bergelin 1952; Drosos *et al.* 2004)

$$Re_\mathrm{f} = 4\frac{\Gamma}{\mu}. \tag{2.8}$$

The factor 4, which arises from consideration of the hydraulic diameter of an infinitely wide falling film (Fulford 1964) is occasionally omitted (e.g. Lel *et al.* 2005; Nogueira *et al.* 2006).

Nusseldt (1916) presents a theoretical analysis of the forces acting on an element of a viscous liquid, falling under gravity, in a film in which the fluid flow is laminar. He derives a solution for the film thickness,

$$\lambda = \left[\frac{3\mu^2}{4\rho^2 g}\, Re_\mathrm{f}\right]^{1/3}. \tag{2.9}$$

Dukler & Bergelin (1952) demonstrate that equation (2.9) is in good agreement with experimental data for $Re_\mathrm{f} \lesssim 1000$, but that it underpredicts film thickness for flow at higher Reynolds number. They conclude that the breakdown of the model is due to the transition to turbulent flow in the falling film, and develop a new theoretical model for the thickness of the film over the laminar-to-turbulent range, based on application of equations originally developed to describe the laminar boundary layer in pipe flow. They propose the following implicit relationship for film thickness:

$$Re_\mathrm{f} = 4\eta(3 + 2.5\ln\eta) - 256, \tag{2.10}$$

where $\eta = \rho\sqrt{g\lambda^3}/\mu$. To test their model, Dukler & Bergelin (1952) perform experiments to determine the thickness of the film falling down a vertical plane surface over the laminar-to-turbulent range ($500 < Re_\mathrm{f} < 3000$). They find that, over this range of Reynolds number, the film thickness varies over time as waves form in the falling film, and that the mean film thickness is in good agreement

with their model (equation (2.10)) across the whole range of Re_f. Fulford (1964) notes that, for thin films, the transition to turbulence occurs over a wider range of flow rates (i.e. a wider range of Reynolds number) than for pipe flow because the boundary layer represents an appreciable fraction of the film thickness, even to relatively high Re_f.

The implicit nature of equation (2.10) limits its practicality, and several experimental studies have sought to determine a more practical correlation for film thickness. Karapantsios *et al.* (1989), Lel *et al.* (2005) and Zhou *et al.* (2009) summarize data from several studies, which use a number of different working fluids and experimental designs. The various datasets, taken together, cover the Reynolds number range $10 \lesssim Re_f \lesssim 15\,000$. Several empirical correlations for film thickness as a function of Reynolds number are presented. The model of Lel *et al.* (2005) is perhaps the most successful in reproducing previous data when $Re_f \lesssim 3000$,

$$\lambda \left[\frac{\rho^2 g}{\mu^2}\right]^{\frac{1}{3}} = 1 + 0.321 Re_f^{0.47}, \tag{2.11}$$

while that of Karapantsios & Karabelas (1995) is more successful when $Re_f \gtrsim 3000$,

$$\lambda \left[\frac{\rho^2 g}{\mu^2}\right]^{1/3} = 0.214 Re_f^{0.538}. \tag{2.12}$$

The models presented above were developed to describe films of liquid falling down vertical surfaces when the film is thin enough that local curvature of the surface can be neglected. In addition to this work, there are several studies that address the thickness of the film falling around a Taylor bubble directly. Goldsmith & Mason (1962) solve the Navier–Stokes equations for laminar flow in a film falling around a Taylor bubble and derive a relationship between the ascent velocity of the bubble and the thickness of the falling film in the thin-film limit

$$v_b = \frac{2\rho g \lambda^3}{3\mu r_c}. \tag{2.13}$$

Brown (1965) extends the analysis of Goldsmith & Mason (1962), relaxing the thin-film assumption to obtain

$$v_b = \frac{2\rho g \lambda^3}{3\mu (r_c - \lambda)}. \tag{2.14}$$

An almost identical result is derived by Batchelor (1967), who considers the balance between viscous and gravitational forces acting on the film; in Batchelor's formulation, the denominator is given by $3\mu(r_c - 2\lambda)$. Under the assumption of a thin liquid film (i.e. $\lambda \ll r_c$), both Brown and Batchelor's expressions reduce to equation (2.13). While Batchelor makes this thin-film assumption, Brown does not, instead adopting a different definition of the Froude number from that

presented in equation (2.1), based on the bubble radius r_b, rather than the pipe radius r_c

$$Fr_B = \frac{v_b}{\sqrt{2gr_b}}. \tag{2.15}$$

Brown further assumes that this Froude number is constant and equal to 0.351, which is the value calculated by Dumitrescu (1943). By substituting this Froude number into equation (2.14), Brown obtains a quadratic, which can be solved for film thickness (eqns 16 and 17 in Brown 1965),

$$\lambda = \frac{\sqrt{1+2Nr_c}-1}{N}, \quad \text{where} \quad N = \left[\frac{16}{9\,Fr_B}\frac{\rho^2 g}{\mu^2}\right]^{1/3}. \tag{2.16}$$

In the last decade, numerical simulations have become sufficiently sophisticated to permit investigation of the rise of Taylor bubbles using 'numerical experiments'. Feng (2008) finds that the thickness of the falling film decreases with increasing Re_b and, equivalently, Taha & Cui (2006) and Kang *et al.* (2010) find that the film thickness decreases with increasing N_f (or Ar where, as previously mentioned, $Ar = N_f^2$). Kang *et al.* go further, performing simulations at $Eo = 200$ and using the data to derive an empirical correlation describing this relationship,

$$\frac{\lambda}{D} = 0.32Ar^{-0.1}. \tag{2.17}$$

This correlation was derived using data from simulations in the range $10^2 < Ar < 2 \times 10^5$.

(*c*) *Falling films: a dimensionless approach*

In this section, we develop a consistent non-dimensionalization for the models presented in §2*b*. For the case of a liquid film falling around a Taylor bubble, it is appropriate to define a dimensionless film thickness $\lambda' = \lambda/r_c$. The physical properties of the liquid and the pipe are encapsulated in the dimensionless inverse viscosity N_f. We show that each of the models for film thickness can be expressed as $\lambda'(N_f)$.

First, we show how the models that were developed for thin films in general (equations (2.9)–(2.12)) can be applied to the case of the film falling around a Taylor bubble. When the film is thin ($\lambda' \to 0$), there is a direct relationship between the film Reynolds number Re_f (equation (2.8)) and the bubble Reynolds number Re_b (equation (2.6)). The downward volume flux of liquid in the film Q_f must balance the upward volume flux of gas in the bubble Q_b; hence, $Q_b = -Q_f$. For a thin film, the liquid flux is given by $Q_f = -\pi D\Gamma/\rho$ and, since $r_b = r_c$ in the limit $\lambda' \to 0$, the gas flux is given by $Q_b = \pi D^2 v_b/4$; hence, $4\Gamma = \rho D v_b$. Dividing through by μ, and noting equations (2.6) and (2.8), we find that, for a thin film, $Re_f = Re_b$.

This equivalence allows straightforward application of the thin-film theory presented in §2*b* to the case of a film falling around a Taylor bubble. The result of Nusseldt (1916) (equation (2.9)) becomes (from equations (2.4) and (2.6))

$$\lambda' = \left[6\frac{Re_b}{N_f^2}\right]^{1/3} = \left[6\frac{Fr}{N_f}\right]^{1/3}. \tag{2.18}$$

Since Fr is a function of N_f only (equation (2.5)), the film thickness predicted by equation (2.18) is also a function of N_f only. Equation (2.18) is valid in the thin-film limit and when flow in the falling film is laminar; the upper limit of applicability of $Re_\mathrm{f} < 1000$ found by Dukler & Bergelin (1952) for equation (2.9) corresponds to an upper limit of $N_\mathrm{f} < 3000$ for equation (2.18) (using equations (2.5) and (2.7)).

The theoretical result of Dukler & Bergelin (1952) (equation (2.10)) for laminar-to-turbulent flow becomes

$$Re_\mathrm{b} = 4\eta(3 + 2.5 \ln \eta) - 256, \tag{2.19}$$

where η can be rewritten in terms of the dimensionless film thickness and the inverse viscosity

$$\eta = N_\mathrm{f} \left[\frac{\lambda'}{2}\right]^{3/2}. \tag{2.20}$$

Since $Re_\mathrm{b} = N_\mathrm{f} Fr$ (equation (2.7)), the film thickness predicted by these equations is a function of N_f only. Dukler & Bergelin (1952) validated equation (2.10) over the range $500 < Re_\mathrm{f} < 3000$, which corresponds to the range $1500 < N_\mathrm{f} < 9000$ for equations (2.19) and (2.20).

The two empirical correlations for the thickness of thin films presented in §2*b* become (equation (2.11); Lel *et al.* 2005)

$$\lambda' = \frac{2 + 0.641\, Re_\mathrm{b}^{0.47}}{\sqrt[3]{N_\mathrm{f}^2}} \tag{2.21}$$

and (equation (2.12); Karapantsios & Karabelas 1995)

$$\lambda' = \frac{0.428\, Re_\mathrm{b}^{0.538}}{\sqrt[3]{N_\mathrm{f}^2}} \tag{2.22}$$

Note that, in both of these expressions, the thickness of the film around a Taylor bubble is a function of N_f only. The experimental support for equation (2.11) over the range $10 < Re_\mathrm{f} < 3000$ and equation (2.12) over the range $3000 < Re_\mathrm{f} < 15\,000$ corresponds to ranges of $40 < N_\mathrm{f} < 9000$ for equation (2.21) and $9000 < N_\mathrm{f} < 44\,000$ for equation (2.22). Equations (2.21) and (2.22) are subject to the additional constraint that the film must be thin.

The models that were developed specifically for films falling around Taylor bubbles (equations (2.13)–(2.17)) can also be expressed as $\lambda'(N_\mathrm{f})$. Goldsmith & Mason (1962) note that their equation relating film thickness and bubble ascent velocity (equation (2.13)) is equivalent to that of Nusseldt (1916) (equation (2.9)); if we rearrange equation (2.13) for λ and divide through by r_c, we do, indeed, recover the dimensionless model that we derived earlier from Nusseldt's model (equation (2.18)). Similarly, under the assumption of a thin liquid film, we can recover equation (2.18) from the expressions of Brown (1965) and Batchelor (1967) (equation (2.14)).

The more general quadratic solution (equation (2.16)) obtained by Brown (1965), which does not make the thin-film assumption, becomes, after dividing through by r_c

$$\lambda' = 2\frac{\sqrt{1 + BN_f^{2/3}} - 1}{BN_f^{2/3}}, \quad \text{where} \quad B = \left[\frac{16}{9\,Fr_B^2}\right]^{1/3} = 2.44. \tag{2.23}$$

As before, film thickness is a function of N_f only. Brown recognizes that the assumption of constant Froude number is not valid when viscosity is important, as this violates Dumitrescu's assumption of potential flow. Brown uses experimental observations of the rise speed of Taylor bubbles to determine a 'viscosity limit' on the validity of his equations, which can be couched in terms of an inverse viscosity condition for validity: $N_f > 120$.

The numerical–empirical model (equation (2.17)) proposed by Kang *et al.* (2010) is already in dimensionless form, and is trivially recast as $\lambda'(N_f)$,

$$\lambda' = 0.64N_f^{-0.2}. \tag{2.24}$$

The range of values of Ar covered by the simulations that underpin this expression leads to a validity range of $10 < N_f < 450$.

Finally, we propose a new model for film thickness, based on that of Brown (1965). Equation (2.14) can be manipulated to produce an expression for the film thickness that avoids both the thin-film assumption and the constant Froude number assumption, hence maintaining validity to small N_f. Noting equations (2.1) and (2.4), we can rearrange equation (2.14) to obtain a depressed cubic for the dimensionless film thickness

$$\lambda'^3 + a\lambda' - a = 0, \quad \text{where} \quad a = 6\frac{Fr}{N_f}, \tag{2.25}$$

which has the rather cumbersome solution

$$\lambda' = \frac{\sqrt[3]{b^2} - \sqrt[3]{12}a}{\sqrt[3]{18b}}, \quad \text{where} \quad b = 9a + \sqrt{12a^3 + 81a^2}. \tag{2.26}$$

Film thickness is a function of N_f only. This result is based upon the assumption of laminar flow, so we expect it to break down when the falling film becomes turbulent; hence, based on the experiments of Dukler & Bergelin (1952), we propose that equation (2.26) should be valid for $N_f < 3000$. We call equations (2.25) and (2.26) the 'Cubic Brown' model.

The seven models for $\lambda'(N_f)$ presented above are summarized in table 1. Each of these models is applicable over different ranges of N_f and the derivation of each model is different. In §4, we test each of these models against experimental data for the thickness of the falling film around rising Taylor bubbles.

(*d*) *The development of the falling film*

The film of liquid falling around a Taylor bubble does not reach its equilibrium thickness until some distance Z behind the nose of the bubble (figure 1). Observations from experiments (Nogueira *et al.* 2006) and numerical simulations

Table 1. Summary of the models presented in §2*c*. Validity ranges are based on previous literature, rather than comparison with data from the current study.

model	equation(s)	source	validity
Nusseldt	(2.18)	Nusseldt (1916)	thin film and $N_f < 3000$
Dukler	(2.19) and (2.20)	Dukler & Bergelin (1952)	$1500 < N_f < 9000$
Lel	(2.21)	Lel *et al.* (2005)	$40 < N_f < 9000$
Karapantsios	(2.22)	Karapantsios & Karabelas (1995)	$9000 < N_f < 44\,000$
Brown	(2.23)	Brown (1965)	laminar film and $N_f > 120$
Kang	(2.24)	Kang *et al.* (2010)	$10 < N_f < 450$
Cubic Brown	(2.25) and (2.26)	new model	laminar film

(Zheng *et al.* 2007; Feng 2008) indicate that this distance depends on the Reynolds number (equivalently, on N_f) and that the length required for the film to develop becomes longer as inertia becomes more important.

Sena Esteves & Guedes de Carvalho (1993) determine an expression for Z. They follow Nicklin *et al.* (1962) and assume that the film is developed when the velocity of the liquid around the nose of the bubble, determined following the potential flow analysis of Dumitrescu (1943), is equal to the velocity at the edge of the falling film, determined following the analysis of Brown (1965). In the thin-film limit, their expression can be written as

$$\frac{Z}{D} = 0.0852(Fr^2 N_f)^{2/3}. \tag{2.27}$$

From equation (2.5) for Fr, we see that the distance Z is a function of N_f only. The assumption of potential flow follows that of Brown (1965); hence, we assume that the expression has the same limit of validity as equation (2.23), i.e. $N_f > 120$. As the analysis also includes the assumption of laminar flow, we expect that it would require modification for transitional and turbulent flow (i.e. for $N_f > 3000$; Dukler & Bergelin 1952). The development length predicted by equation (2.27) for these lower and upper limits of N_f is, respectively, $Z = 0.4D$ and $4.1D$.

The approach to equilibrium film thickness for transitional and turbulent films has been investigated experimentally (Takahama & Kato 1980; Karapantsios & Karabelas 1995), although neither of these studies specifically considers the film around Taylor bubbles. The results are complex and no general model is developed. Nogueira *et al.* (2006) perform experiments with Taylor bubbles in the range $2 < Re_b < 6000$ ($15 < N_f < 18\,000$) and adopt an expression for Z proposed by Campos & Guedes de Carvalho (1988), which is based on similar assumptions to those that underpin equation (2.27). They find that this approach underpredicts film thickness at low Reynolds number, and overpredicts at high Reynolds number; they conclude that flow undergoes the transition from laminar to turbulent for $Re_b > 320$ ($N_f > 1000$). Zheng *et al.* (2007) perform numerical simulations of the rise of Taylor bubbles over the laminar-to-turbulent range ($90 < N_f < 21\,000$), using a volume-of-fluid approach that includes a k–ϵ

turbulence model. They find that the film develops to its equilibrium thickness at $1.5 < Z/D < 2.1$, which is rather smaller than the value predicted by the laminar model (equation (2.27)) at its upper validity limit.

3. Laboratory experiments and data analysis

Quantitative experimental data for the equilibrium thickness of the falling film around a rising Taylor bubble are scarce, and we are aware of only one systematic study: that of Nogueira *et al.* (2006). They image the flow around Taylor bubbles of air rising up a pipe with $r_c = 0.016\,\mathrm{m}$, filled with liquids with viscosities in the range $10^{-3} < \mu < 1.5\,\mathrm{Pa\,s}$, and with densities close to that of water. Their experiments span the range $15 < N_f < 18\,000$ and, assuming appropriate values for the interfacial tension, we infer that the Eötvös number is in the range $140 < Eo < 200$ (note that, while they investigate the rise of Taylor bubbles through both stagnant and concurrently flowing columns of water, we consider only their results for the stagnant case). While their experiments cover a wide range of inverse viscosity, they do not collect data for sufficiently low values of N_f to constrain behaviour in the viscous, thick-film regime; hence, their data are not suitable to test the validity of the Nusseldt and Brown models (see §2*c* and table 1) at low N_f. Furthermore, Nogueira *et al.* use only a single pipe diameter and cover a narrow range of Eo; consequently, additional data are also required to provide a more exacting test of the non-dimensionalizations (to N_f and λ').

We conducted laboratory experiments in which Taylor bubbles were formed by introducing air into cylindrical, transparent acrylic pipes of three different internal radii ($r_c = 0.01$, 0.02, 0.04 m) and of length 2 m. The pipes were filled with a variety of Newtonian liquids (golden syrup, cooking oil, liquid soap, water and mixtures prepared by diluting syrup or soap with water) in order to cover a range of values of viscosity and interfacial tension. Stress–strain rate flow curves were determined with a rotational rheometer at controlled ambient temperature, and all liquids were found to have Newtonian rheology. Data from five repeat runs were used to determine viscosity μ with a typical error of less than 0.5 per cent; however, owing to small temperature fluctuations during experiments, we put a conservative uncertainty of 5 per cent on viscosity. The density of each liquid was measured by weighing a known volume at controlled ambient temperature with error in ρ of less than 1 per cent. The interfacial tension of cooking oil, soap and soap solutions was measured using the drop shape method (Adamson 1990) with an error in σ of less than 10 per cent. The interfacial tension of pure and diluted golden syrup was taken from Llewellin *et al.* (2002). Measured physical properties of the liquids are presented in table 2.

Taylor bubbles were formed by partially filling the pipes with liquid to leave an air pocket of length L_0, then sealing and inverting the pipe (a similar method was employed by Niranjan *et al.* 1988). The Taylor bubble's ascent was recorded in the upper part of the pipe using high-definition videography (Casio Exilim EX-F1). After each ascent, liquid was added and the experiment was re-run; between 8 and 16 different values of L_0 were used for each liquid/pipe combination (typically covering the range $0.01 \lesssim L_0 \lesssim 0.3\,\mathrm{m}$), thus producing a suite of n data points for each value of N_f. The experimental apparatus and several example images of Taylor bubbles are presented in figure 2.

Table 2. Experimental results. Dilutions of syrup and soap are indicated by 'd1' and 'd2'.

liquid	μ (Pa s)	ρ (kg m^{-3})	σ (N m^{-1})	r_c (m)	n	v_b (m s^{-1})	σ_{v_b} (m s^{-1})	β	σ_β	Fr	λ'	Eo	N_f
syrup	4.0×10^{1}	1390	0.080	0.0956	8	0.00117	2.81×10^{-5}	2.13	2.34×10^{-2}	0.00269	0.314	62	2.86×10^{-1}
syrup d1	3.7×10^{0}	1370	0.080	0.0956	8	0.0124	8.44×10^{-4}	2.18	2.28×10^{-2}	0.0286	0.323	61	3.07×10^{0}
syrup d2	1.2×10^{0}	1360	0.080	0.0956	8	0.0380	5.91×10^{-4}	2.16	2.01×10^{-2}	0.0878	0.319	61	9.79×10^{0}
soap	3.3×10^{-1}	1027	0.020	0.01	14	0.0944	3.06×10^{-3}	2.07	2.06×10^{-2}	0.213	0.305	202	2.76×10^{1}
soap d1	1.7×10^{-1}	1019	0.035	0.01	14	0.136	1.17×10^{-3}	1.86	2.88×10^{-2}	0.308	0.267	114	5.28×10^{1}
soap	3.3×10^{-1}	1027	0.020	0.02	10	0.187	1.96×10^{-3}	1.85	2.26×10^{-2}	0.299	0.266	806	7.80×10^{1}
soap d1	1.7×10^{-1}	1019	0.035	0.02	8	0.205	1.28×10^{-3}	1.66	4.65×10^{-2}	0.328	0.225	457	1.49×10^{2}
oil	4.6×10^{-2}	895	0.032	0.01	11	0.142	1.08×10^{-3}	1.59	1.40×10^{-2}	0.320	0.207	110	1.74×10^{2}
soap	3.3×10^{-1}	1027	0.020	0.04	13	0.286	2.80×10^{-3}	1.50	1.36×10^{-2}	0.322	0.184	3230	2.21×10^{2}
soap d1	1.7×10^{-1}	1019	0.035	0.04	11	0.313	2.19×10^{-3}	1.41	8.86×10^{-3}	0.353	0.158	1830	4.22×10^{2}
oil	4.6×10^{-2}	895	0.032	0.02	12	0.206	2.45×10^{-3}	1.43	2.57×10^{-2}	0.329	0.163	439	4.92×10^{2}
soap d2	1.5×10^{-2}	1009	0.045	0.01	15	0.148	7.46×10^{-4}	1.36	1.59×10^{-2}	0.334	0.142	88	5.96×10^{2}
oil	4.6×10^{-2}	895	0.032	0.04	14	0.324	6.69×10^{-3}	1.34	1.67×10^{-2}	0.366	0.135	1760	1.39×10^{3}
soap d2	1.5×10^{-2}	1009	0.045	0.02	8	0.227	1.93×10^{-3}	1.19	2.31×10^{-2}	0.362	0.0817	352	1.69×10^{3}
soap d2	1.5×10^{-2}	1009	0.045	0.04	12	0.293	2.90×10^{-3}	1.17	3.47×10^{-2}	0.331	0.0758	1410	4.77×10^{3}
water	1.2×10^{-3}	1000	0.073	0.01	15	0.149	1.56×10^{-3}	1.17	1.22×10^{-2}	0.337	0.0737	54	7.38×10^{3}
water	1.2×10^{-3}	1000	0.073	0.02	12	0.216	2.22×10^{-3}	1.19	1.04×10^{-2}	0.345	0.0838	215	2.09×10^{4}
water	1.2×10^{-3}	1000	0.073	0.04	16	0.305	1.77×10^{-3}	1.20	1.19×10^{-2}	0.344	0.0860	860	5.90×10^{4}

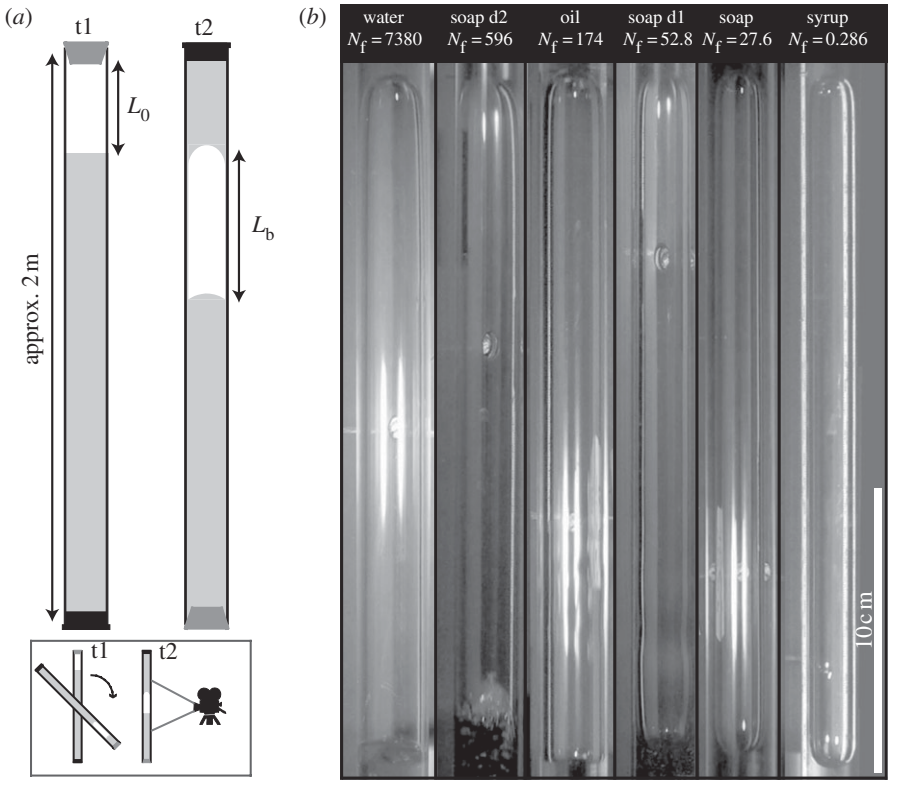

Figure 2. (*a*) Experimental set-up. For each experimental run, a progressively decreasing amount of air was left in the pipe by adding fixed volumes of liquid (t1). The pipe was inverted, resulting in the formation of Taylor bubbles with different length. The bubble's ascent was captured using a high-definition video camera (t2). (*b*) Taylor bubbles rising through various liquids in a pipe with $r_c = 0.01$ m; images are arranged with N_f decreasing from left to right. Physical properties of the liquids are given in table 2.

4. Results

(*a*) *Shape and ascent velocity of bubbles*

Consistent with previous studies, discussed in §1, we find that the shapes of the nose and body of the bubble are qualitatively the same for all bubbles, and are independent of bubble length and other experimental parameters. The morphology of the tail and the nature of the wake that follows it vary systematically with inverse viscosity, as previously shown in both laboratory experiments (Campos & Guedes de Carvalho 1988; Viana *et al.* 2003) and numerical simulations (Kang *et al.* 2010). We find that the shape of the tail is stable for $N_f \lesssim 600$ and unstable for $N_f \gtrsim 600$, as reported by Campos & Guedes de Carvalho (1988).

Video images were analysed using the freely available ImageJ software, and the ascent velocity v_b and the length of the bubble L_b were recorded. The velocity was determined by measuring the position of the bubble's nose in two frames of the video (near the bottom and top of the measurement section, respectively)

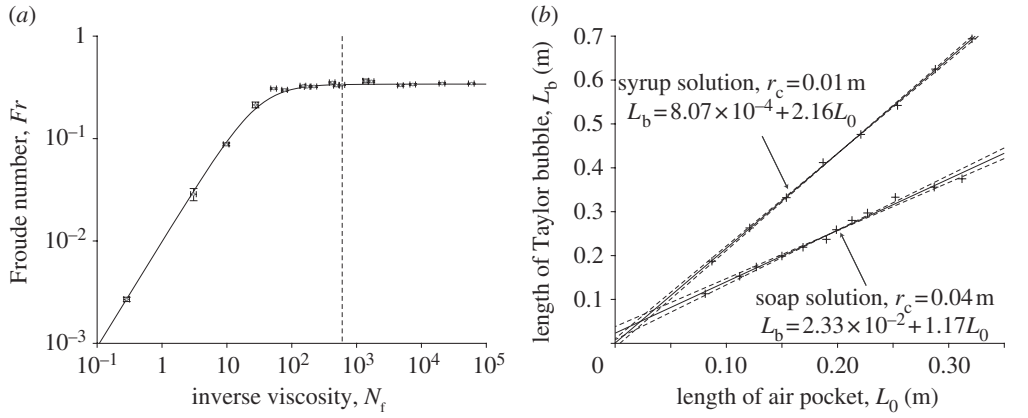

Figure 3. (*a*) Experimentally determined Froude number (equation (2.1)) plotted against inverse viscosity (equation (2.4)); solid line is the empirical expression for $Fr(N_f)$ of Viana *et al.* (2003) (equation (2.5)); vertical line marks the observed transition from stable to unstable tail shape. (*b*) Relationship between bubble length L_b and initial length of the air pocket L_0 for two suites of data (i.e. two values of N_f). In general, we find a relationship of the form $L_b = \alpha + \beta L_0$, where $\beta = (1-\lambda')^{-2}$; best-fit values of β (solid lines) and 95% confidence limits on β (dashed lines) are computed. The two suites plotted are chosen to demonstrate the best (syrup solution) and worst (soap solution) agreement with a linear model.

and noting the elapsed time. For each value of N_f, velocity was determined for all of the bubbles in the suite of data, and was found to be independent of bubble length. The mean value of v_b was calculated for each suite, along with the standard deviation σ_{v_b}. These data were used to compute Froude number (equation (2.1)), and results are plotted against N_f in figure 3*a*. The empirical expression for $Fr(N_f)$ of Viana *et al.* (2003) (equation (2.5)) is also plotted, and shows excellent agreement with the experimental data. Error in Fr is determined from $2\sigma_{v_b}$ and a conservative compound error of $\pm 10\%$ in N_f is determined from the errors in ρ, μ and D.

The length of each bubble from nose to tail, L_b, was measured from a single video frame and was plotted against L_0 for each suite of data; two examples are shown in figure 3*b*. A linear relationship between L_b and L_0 was found for every suite,

$$L_b = \alpha + \beta L_0, \quad \text{where} \quad \beta = (1-\lambda')^{-2} \tag{4.1}$$

and α is a constant related to the length of the nose and tail regions. This linearity indicates that only the cylindrical part of the body of the bubble (2b in figure 1) changes length as gas volume changes, the nose, upper body and tail remaining unchanged; hence, the thickness of the falling film in the cylindrical part of the body region is, indeed, independent of bubble length. Similar data are presented by Nicklin *et al.* (1962, fig. 2) for experiments at a single inverse viscosity ($N_f \approx 12\,000$). They plot $(L_b - L_0)$ against L_b and also find a straight line relationship, where their gradient β_N is related to ours (β) by $\beta_N = 1 - 1/\beta = 2\lambda'(1-\lambda')$. Nicklin and co-workers observe that, for their experimental conditions, the linearity between $(L_b - L_0)$ and L_b is broken for very short bubbles ($L_b < 6D$) because the bubbles are insufficiently long for the falling film to develop

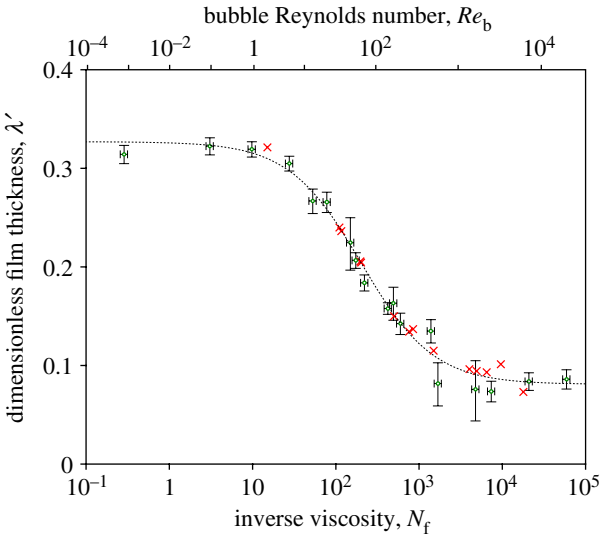

Figure 4. Experimentally determined values of λ' plotted against inverse viscosity (equation (2.4)) and bubble Reynolds number (equations (2.5) and (2.7)). Circles are data from this study with error bars computed as described in §4; crosses are data for the rise of Taylor bubbles up a stagnant column of liquid taken from table 1 of Nogueira *et al.* (2006). The dotted line is the best fit of a purely empirical model (equation (4.2)) described in the text. (Online version in colour.)

to equilibrium thickness (i.e. $L_b < Z$; §2*d*). We find that the linearity holds for all L_b in our experiments, indicating that all of the bubbles we investigate are sufficiently long for equilibrium to have been reached.

(*b*) *Thickness of the falling film*

For each data suite (i.e. for each value of N_f), the best-fit value of β was found by linear regression of equation (4.1). The standard deviation σ_β was then calculated (assuming that errors in the residual are normally distributed) and, from these data, 95% confidence limits on β were computed. These values were used to determine λ' and upper and lower bounds on λ'. Results are summarized in table 2.

Results are also plotted in figure 4. The figure shows that film thickness is a strong function of inverse viscosity; it also demonstrates that all the data collapse to a single curve, indicating that the non-dimensionalizations (of film thickness to λ', and of material properties and pipe diameter to N_f) are appropriate, and are sufficient to characterize the system when surface tension can be neglected ($Eo > 40$; see §2*a*).

The data show a clear, sigmoidal trend in $\lambda'(\log_{10} N_f)$: for $N_f \lesssim 10$, the dimensionless film thickness is independent of N_f with value $\lambda' \approx 0.33$; in the interval $10 \lesssim N_f \lesssim 10^4$, λ' decreases with increasing N_f; for $N_f \gtrsim 10^4$, film thickness is, again, independent of N_f with value $\lambda' \approx 0.08$. Based on the observed sigmoidal relationship, we propose the following empirical model:

$$\lambda' = a + b \tanh(c - d \log_{10} N_f), \tag{4.2}$$

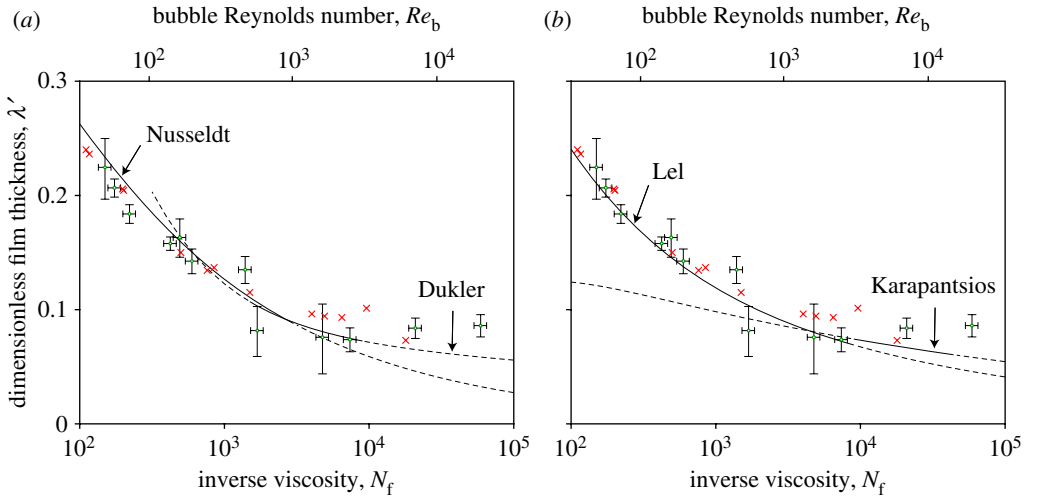

Figure 5. High-N_f subset of the data presented in figure 4, used to assess the validity of four models appropriate for the thin-film regime: (*a*) the Nusseldt model and the Dukler model and (*b*) the Lel model and the Karapantsios model (see table 1). Each of the models is presented as a solid line within its validity range, and as a dashed line outside this range. (Online version in colour.)

where the values of the four constants $a = 0.204$, $b = 0.123$, $c = 2.66$ and $d = 1.15$, are determined by fitting to the combined data from this study and from Nogueira *et al.* (2006). Despite the empirical nature of the model, the parameters can be mapped to their physical meaning: the low-N_f and high-N_f asymptotic values of λ' are given by $a + b$ and $a - b$, respectively; c describes the position of the transition between these asymptotes; and d describes how abrupt the transition is. The model gives an excellent fit to the experimental data across the measurement range of N_f, and is discussed further in §5*c*.

5. Discussion

(*a*) *Thin films and the transition to turbulence*

Figure 5 plots a high-N_f subset of the data presented in figure 4, and compares it with models for film thickness appropriate for the thin-film regime. The comparison is presented over two sub-figures for clarity.

Figure 5*a* shows the two theoretical models for film thickness that were derived from consideration of thin films falling down plane surfaces: the Nusseldt model (equation (2.18)) for laminar films and the Dukler model (equation (2.19)) for films over the laminar-to-turbulent transition. The Nusseldt model shows an excellent agreement with the experimental data for $N_f \lesssim 3000$. The Dukler model is in good agreement with the data for $500 \lesssim N_f \lesssim 20\,000$, which extends the range of validity beyond that claimed by Dukler & Bergelin (1952). The failure of the Nusseldt model for laminar flow at $N_f > 3000$ echoes the findings of Dukler & Bergelin (1952), whose experimental data confirmed Nusseldt's theory for films falling down a plane surface (equation (2.9)) for $Re_f < 1000$. This result supports the validity of our approach in adapting thin-film theory (§2*b*) to the case of films

around Taylor bubbles, presented in §2*c*. Dukler & Bergelin (1952) attribute the failure of the Nusseldt model for $Re_b > 1000$ to the onset of flow transition in the film; consequently, we put the laminar-to-turbulent transition at $N_f \approx 3000$. We note that this is rather higher than the value proposed by Nogueira *et al.* (2006), which can be couched as $N_f \approx 1000$.

Figure 5*b* shows the two empirical models for film thickness that were derived from data for thin films falling down plane surfaces: the Lel model (equation (2.21)) and the Karapantsios model (equation (2.22)). The Lel model shows excellent agreement with the data within its range of validity (table 1). The Karapantsios model shows reasonable agreement over the range $2000 \lesssim N_f \lesssim 20\,000$.

There is poor agreement between our data and the Dukler and Karapantsios models for $N_f \gtrsim 20\,000$, despite the fact that both were developed for falling films at high Reynolds number. The experimentally determined film thickness is greater than the model thickness; however, we note that this trend is based on a small number of data points. There are two possible causes for this discrepancy.

The first possibility is that the experimental data are unreliable at large N_f, either because the falling film was not fully developed in these experiments, or because gas entrainment from the Taylor bubble into the wake during ascent was significant. The linear relationship between L_b and L_0 observed for all of our experiments (§4*a*), including those at the highest values of N_f, leads us to conclude that there was negligible variation in film thickness over the range of bubble lengths investigated. This observation, combined with the numerical results of Zheng *et al.* (2007) (discussed in §2*d*), which indicate short development lengths for turbulent falling films, leads us to conclude that the films were fully developed in our experiments. Visual observation of the bubbles during ascent suggests that gas entrainment into the wake is insignificant; furthermore, we note that the same discrepancy between data and models at high N_f is present for the data of Nogueira *et al.* (2006), who measure film thickness directly.

The second possibility is that the models are not appropriate for high N_f conditions; we note that our highest N_f values are outside the validity ranges of both the Dukler and Karapantsios models. The failure of the theoretical Dukler model to agree with the data could indicate that some assumption of that model is violated at very high N_f. Alternatively, it is possible that the analogy between thin films falling down plane surfaces, and thin films falling around Taylor bubbles, which underpins the analysis at the start of §2*c*, breaks down at very high N_f. Further work is required to address these issues at very high N_f.

(*b*) *Intermediate and thick films*

Figure 6 compares the data presented in figure 4 with models for film thickness that are appropriate for intermediate and low values of N_f. The comparison is presented over two sub-figures for clarity.

Figure 6*a* shows that the Kang model (equation (2.24)), which is based on an empirical fit to data from numerical simulations, is generally in poor agreement with laboratory experimental data, except over a very narrow range of N_f. The Brown model (equation (2.23)) performs rather better, agreeing closely with the data in the range $50 \lesssim N_f \lesssim 3000$; however, as the Brown model reduces to the Nusseldt model (equation (2.18)) in the thin-film limit, it shows the same poor fit

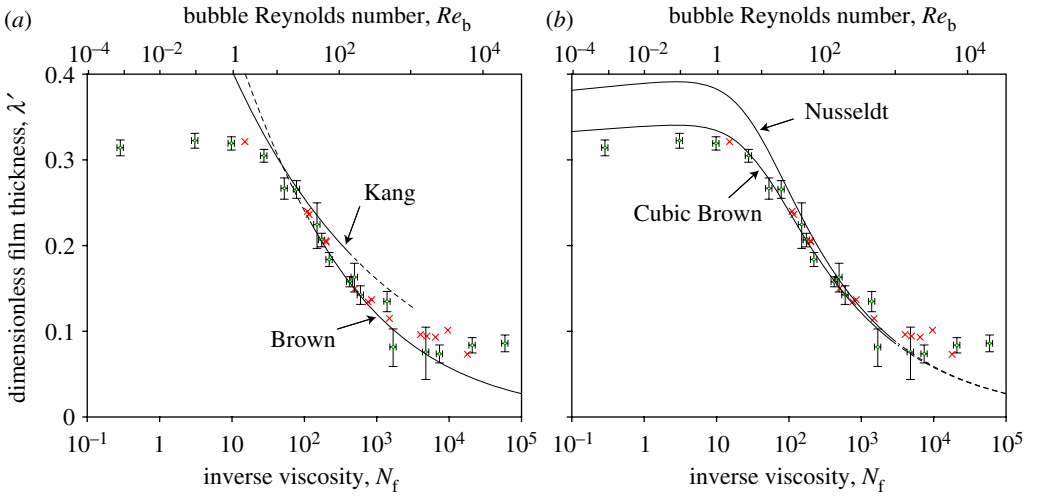

Figure 6. Comparison of the data presented in figure 4 with four models appropriate for intermediate and low values of N_f: (*a*) the Brown model and the Kang model and (*b*) the Nusseldt model and the Cubic Brown model (see table 1). Each of the models is presented as a solid line within its validity range, and as a dashed line outside this range. (Online version in colour.)

to data at high N_f (described in §5*a*). The Brown model differs from the Nusseldt model (figure 6*b*) in two ways. Firstly, it has the advantage that it does not include the thin-film assumption, which explains its better agreement with data at intermediate N_f than the Nusseldt model. Secondly, however, the Brown model assumes constant Froude number (Fr_B), which explains its poor performance at low N_f, where the Froude number is a strong function of N_f (equation (2.5)). This weakness of the model was acknowledged by Brown, who put the lower limit of validity for the model at $N_f > 120$ as a consequence. In our formulation of the Nusseldt model, we calculate the Froude number using the model of Viana *et al.* (2003) (equation (2.5)), hence its better performance than the Brown model at low N_f.

The new model that we propose, the Cubic Brown model (equations (2.25) and (2.26)), shows an excellent fit to data for $N_f \lesssim 3000$ (figure 6*b*). This model combines the best features of the Brown and the Nusseldt models, in that it relaxes the thin-film assumption while allowing the Froude number to vary as a function of N_f. Comparing the Nusseldt and the Cubic Brown model curves allows the impact of the thin-film assumption to be assessed, as this is the only difference between the models; the divergence between the predictions of the two models is appreciable only for $N_f \lesssim 200$, implying that the film can be considered 'thin' for inverse viscosities above this value. The price for the superior performance of the Cubic Brown model is that it is rather more complex than both the Brown and the Nusseldt models.

(*c*) *A general model for film thickness*

Based on the discussion above, we propose two general models for the thickness of the falling film around a rising Taylor bubble in the case where interfacial

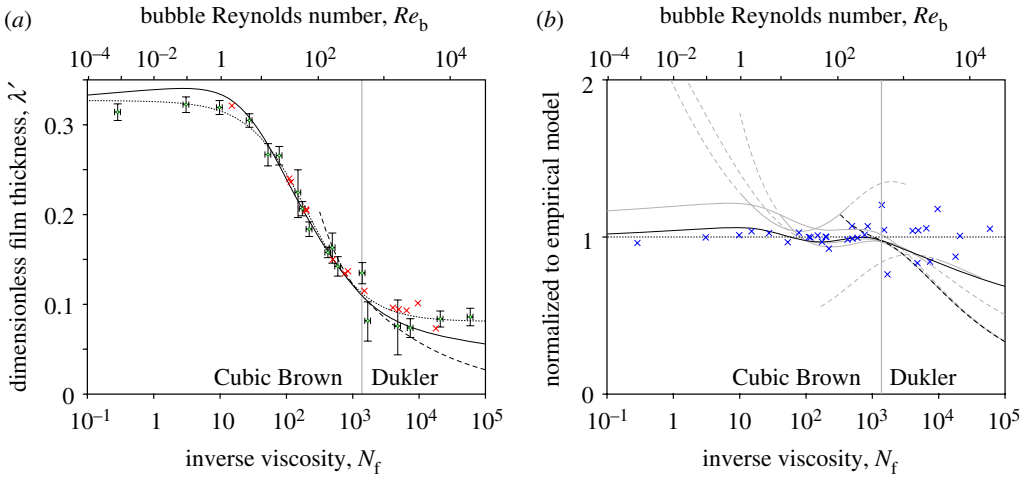

Figure 7. (*a*) Comparison of the preferred theoretical (solid lines) and empirical models (dotted lines) discussed in §5*c* with the data presented in figure 4. The Cubic Brown model is the preferred theoretical model for $N_f \leq 1372$; for $N_f > 1372$, the Dukler model is preferred. (*b*) The value of film thickness predicted by each of the models presented in table 1 is normalized by the value predicted by the empirical model, equation (4.2). The preferred theoretical models are presented as a solid black line, the other models in table 1 are presented as grey lines. The crosses in (*b*) are the combined data from this study and those of Nogueira *et al.* (2006). (Online version in colour.)

tension is negligible. The first model has a sound theoretical underpinning, the second is purely empirical. Figure 7*a* compares both models with the experimental data from figure 4.

The theoretical model is composed of two parts: for low and intermediate values of N_f, the film thickness is given by the Cubic Brown model (equations (2.25) and (2.26)); for high N_f, it is given by the Dukler model (equations (2.19) and (2.20)). This combined model gives a good fit to data across the range $0.1 < N_f < 20\,000$. However, it does have three drawbacks. (i) It is discontinuous. There is no value of N_f for which the Cubic Brown and the Dukler models give exactly the same value of λ'. The closest approach between the two occurs when $N_f = 1372$, at which value, the difference is just 0.3 per cent. This provides a natural point at which to switch between the two models; hence, we propose that the Cubic Brown model is used for $N_f \leq 1372$ and the Dukler model is used for $N_f > 1372$. (ii) It is cumbersome, and involves multiple calculation steps. For example, to calculate λ', we first calculate N_f from equation (2.4). If $N_f \leq 1372$, then the Froude number is calculated using the empirical relationship of Viana *et al.* (2003) (equation (2.5)), then a, b and finally λ' are calculated from equations (2.25) and (2.26); if $N_f > 1372$, η is calculated using equation (2.20), then λ' must be evaluated from the implicit equation (2.19) (for this study, the implicit equation was solved using a standard spreadsheet solver function). (iii) The model underpredicts the film thickness for $N_f > 20\,000$. Despite these shortcomings, we recommend that this model is used when an approach with a sound theoretical underpinning is desired; the only empirical element is the Froude number calculation required when $N_f < 1372$.

The empirical model is given by equation (4.2). This is based on a purely empirical fit to the combined data from this study and from Nogueira *et al.* (2006). The functional form was chosen based on the observation that λ' shows a sigmoidal dependence on $\log_{10} N_f$. This model has the advantage that it gives an excellent fit to the data across the six orders of magnitude of inverse viscosity investigated ($0.1 < N_f < 10^5$). A disadvantage of the empirical model is that it has no theoretical underpinning, so extrapolation outside the empirically validated range of N_f is not recommended.

In figure 7*b*, the value of λ' predicted by each of the models presented in table 1 is normalized by the value predicted by the empirical model (equation (4.2)). This allows the relative accuracy of each model to be assessed across the range of N_f investigated.

(*d*) *Film thickness when interfacial tension is not negligible*

This study has focussed on the behaviour of Taylor bubbles in the case where interfacial tension is negligible. According to Viana *et al.* (2003), interfacial tension can be neglected when $Eo > 40$, which is the case for all of the data collected in this study, and in that of Nogueira *et al.* (2006). The nature of the new theoretical model that we develop in §2*c* (the Cubic Brown model; equations (2.25) and (2.26)) allows us tentatively to generalize the model to the case where interfacial tension cannot be neglected.

The Froude number that enters into the Cubic Brown model via equation (2.16) for a is calculated from equation (2.5), which is a simplified form of the more general empirical correlation for Froude number developed by Viana *et al.* (2003). That general correlation allows the Froude number to be determined when interfacial tension is important ($6 < Eo < 40$). In figure 8, we calculate the film thickness using the Cubic Brown model, but take the Froude number from the general correlation of Viana *et al.* (2003, eqn (23)) for a range of different values of Eo.

The results show that the film thickness is strongly dependent on Eo for $Eo < 40$, and that the dependence is more pronounced for smaller values of N_f (or, equivalently, for thicker films). Film thickness decreases as the role of interfacial tension becomes more important (i.e. as Eo decreases). For $Eo < 4$, Taylor bubbles should not form because capillary forces prevent the bubble from rising (White & Beardmore 1962). Results are not plotted for $N_f > 1372$ because interfacial tension may play a different role in controlling film thickness for transitional and turbulent films (see Drosos *et al.* 2004 for a discussion of the role, in such films, of the Kapitza number, which is the inverse cube root of the Morton number).

While the proposed approach is speculative—it is not clear that the theoretical approach of Brown (1965) is valid without additional modification when interfacial tension is important—our data offer some empirical support for the trend of decreasing film thickness with decreasing Eo. The data points at the three lowest values of N_f were collected under conditions where $Eo \approx 60$, i.e. only just above the threshold above which Viana *et al.* (2003) claim that Fr is independent of Eo. In fact, the curves in figure 8 demonstrate that film thickness is still dependent on Eo, albeit mildly, for $Eo > 40$. Consequently, these three data points plot very close to the theoretical value that is predicted for $Eo = 60$, supporting our approach.

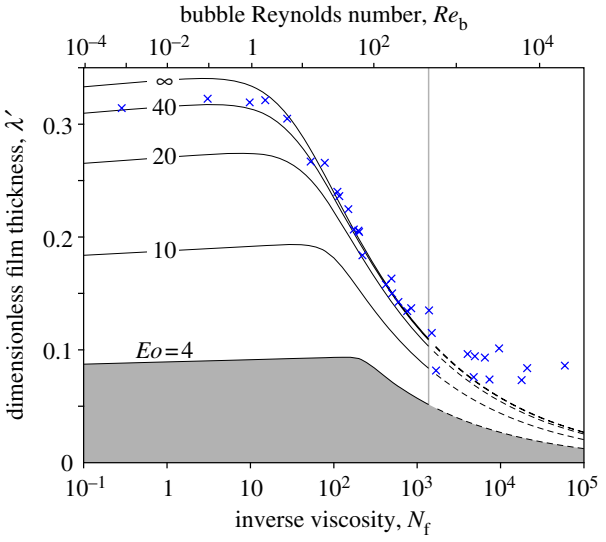

Figure 8. Dimensionless film thickness when interfacial tension cannot be neglected. Solid lines represent the prediction of the Cubic Brown model when the value of Fr is computed using the full model of Viana *et al.* (2003, eqn (23)) for various values of Eo. The crosses are the combined data from this study and those of Nogueira *et al.* (2006). The lines are dashed outside their region of validity. In the shaded region, capillary forces are expected to prevent bubbles from rising. (Online version in colour.)

6. Conclusions

Our theoretical analysis and experimental data demonstrate that, in the case where interfacial tension can be ignored ($Eo > 40$, equation (2.3)), the thickness of the film of liquid that falls around a rising Taylor bubble is a function of the inverse viscosity only (N_f; equation (2.4)). Previous studies that have identified the Reynolds number Re_b as the key parameter (Nogueira *et al.* 2006; Feng 2008) are consistent with our findings, as we have demonstrated that Re_b is a function of N_f only. We propose that N_f is a more practical parameter because it is computed simply from the material and geometric properties of the system. Our experiments show that the dimensionless film thickness λ' has a sigmoidal dependence on $\log_{10} N_f$ (figure 4). For $N_f \lesssim 10$, the dimensionless film thickness is independent of N_f with value $\lambda' \approx 0.33$; in the interval $10 \lesssim N_f \lesssim 10^4$, λ' decreases with increasing N_f; for $N_f \gtrsim 10^4$, film thickness is, again, independent of N_f with value $\lambda' \approx 0.08$. Our data are the first to cover a sufficiently wide range of N_f to constrain the asymptotic values of λ'.

We propose two models for the dimensionless film thickness as a function of inverse viscosity (§5*c*). The first model is based on theory, and is split into two parts: for $N_f \leq 1372$, where flow in the film is laminar, we propose a new relationship for film thickness (equations (2.5), (2.25) and (2.26)), which we develop from the analyses of Brown (1965) and Viana *et al.* (2003); for $N_f > 1372$, where flow in the film spans the laminar-to-turbulent transition, we propose a version of the theory of Dukler & Bergelin (1952) (equations (2.19) and (2.20)), which was originally developed for falling films in general, and which we adapt for

the specific case of a thin film falling around a Taylor bubble. This two-part model shows good agreement with experimental data in the range $0.1 < N_f < 20\,000$. By comparing our model with previous work, and with our data, we conclude that the commonly made 'thin-film' assumption is valid only for $N_f > 200$. The second model is a purely empirical correlation (equation (4.2)), which is based on a fit to data collected in this study and by Nogueira *et al.* (2006). It provides an excellent fit to data in the range $0.1 < N_f < 100\,000$.

Finally, we propose a method for calculating film thickness when interfacial tension cannot be neglected (§5*d*). This analysis suggests that films become thinner as interfacial tension becomes more important.

We thank the staff of the HP-HT Laboratory at INGV Roma (Seismology and Tectonophysics) who contributed to the experimental work in the Laboratory of Experimental Volcanology and Geophysics, in particular, we are grateful to Massimo Mari for technical support in developing the experimental set-up and to Pierdomenico Del Gaudio and Silvio Mollo for assistance during laboratory measurements. We are also grateful to two anonymous reviewers of this manuscript, and to two anonymous reviewers of an earlier version.

References

Adamson, A. W. 1990 *Physical chemistry of surfaces*, 5th edn. New York, NY: John Wiley & Sons Inc.

Amaya-Bower, L. & Lee, T. 2011 Numerical simulation of single bubble rising in vertical and inclined square channel using lattice Boltzmann method. *Chem. Eng. Sci.* **66**, 935–952. (doi:10.1016/j.ces.2010.11.043)

Batchelor, G. K. 1967 *An introduction to fluid dynamics*. Cambridge, UK: Cambridge University Press.

Blackburn, E. A., Wilson, L. & Sparks, R. S. J. 1976 Mechanisms and dynamics of strombolian activity. *J. Geol. Soc. Lond.* **132**, 429–440. (doi:10.1144/gsjgs.132.4.0429)

Brown, R. A. S. 1965 Mechanics of large gas bubbles in tubes. I. Bubble velocities in stagnant liquids. *Can. J. Chem. Eng.* **43**, 217–223. (doi:10.1002/cjce.5450430501)

Bugg, J. D. & Saad, G. A. 2002 The velocity field around a Taylor bubble rising in a stagnant viscous fluid: numerical and experimental results. *Int. J. Multiphase Flow* **28**, 791–803. (doi:10.1016/S0301-9322(02)00002-2)

Bugg, J. D., Mack, K. & Rezkallah, K. S. 1998 A numerical model of Taylor bubbles rising through stagnant liquids in vertical tubes. *Int. J. Multiphase Flow* **24**, 271–281. (doi:10.1016/S0301-9322(97)00047-5)

Campos, J. B. L. M. & Guedes de Carvalho, J. R. F. 1988 An experimental study of the wake of gas slugs rising in liquids. *J. Fluid Mech.* **196**, 27–37. (doi:10.1017/S0022112088002599)

Chouet, B., Dawson, P., Ohminato, T., Martini, M., Saccorotti G., Giudicepietro F., De Luca, G., Milana, G. & Scarpam R. 2003 Source mechanisms of explosions at Stromboli Volcano, Italy, determined from moment–tensor inversions of very-long-period data. *J. Geophys. Res.* **108**, 2019. (doi:10.1029/2002JB001919)

Chouet, B., Dawson, P., James, M. R. & Lane, S. J. 2010 Seismic source mechanism of degassing bursts at Kilauea Volcano, Hawaii: results from waveform inversion in the 10–50 s band. *J. Geophys. Res.* **115**, B09311. (doi:10.1029/2009JB006661)

Davies, R. M. & Taylor, G. 1950 The mechanics of large bubbles rising through extended liquids and through liquids in tubes. *Proc. R. Soc. Lond. A* **200**, 375–390. (doi:10.1098/rspa.1950.0023)

Del Bello, E., Llewellin, E. W., Taddeucci, J., Scarlato, P. & Lane, S. J. Accepted. An analytical model for gas overpressure in slug-driven explosions: insights into strombolian volcanic eruptions. *J. Geophys. Res.*

Drosos, E. I. P., Paras, S. V. & Karabelas, A. J. 2004 Characteristics of developing free falling films at intermediate Reynolds and high Kapitza numbers. *Int. J. Multiphase Flow* **30**, 853–876. (doi:10.1016/j.ijmultiphaseflow.2004.03.003)

Dukler, A. E. & Bergelin, O. P. 1952 Characteristics of flow in falling liquid films. *Chem. Eng. Prog.* **48**, 557–563.

Dumitrescu, D. T. 1943 Strömung an einer Luftblase im senkrechten Rohr. *Z. Angew. Math. Mech.* **23**, 139–149. (doi:10.1002/zamm.19430230303)

Fabré, J. & Liné, A. 1992 Modeling of two-phase slug flow. *Annu. Rev. Fluid Mech.* **24**, 21–46. (doi:10.1146/annurev.fl.24.010192.000321)

Feng, J. Q. 2008 Buoyancy-driven motion of a gas bubble through viscous liquid in a round tube. *J. Fluid Mech.* **609**, 377–410. (doi:10.1017/S0022112008002516)

Fulford, G. D. 1964 The flow of liquids in thin films. *Adv. Chem. Eng.* **5**, 151–236. (doi:10.1016/S0065-2377(08)60008-3)

Funada, T., Joseph, D. D., Maehara, T. & Yamashita, S. 2005 Ellipsoidal model of the rise of a Taylor bubble in a round tube. *Int. J. Multiphase Flow* **31**, 473–491. (doi:10.1016/j.ijmultiphaseflow.2004.11.010)

Goldsmith, H. L. & Mason, S. G. 1962 The movement of single large bubbles in closed vertical tubes. *J. Fluid Mech.* **14**, 42–58. (doi:10.1017/S0022112062001068)

James, M. R., Lane, S. J. & Chouet, B. 2006 Gas slug ascent through changes in conduit diameter: laboratory insights into a volcano-seismic source process in low-viscosity magmas. *J. Geophys. Res.* **111**, B05201. (doi:10.1029/2005JB003718)

James, M. R., Lane, S. J. & Wilson, L. 2009 Degassing at low magma-viscosity volcanoes: quantifying the transition between passive bubble-burst and strombolian eruption. *J. Volcanol. Geotherm. Res.* **180**, 81–88. (doi:10.1016/j.jvolgeores.2008.09.002)

Kang, C. W., Quan, S. P. & Lou, J. 2010 Numerical study of a Taylor bubble rising in stagnant liquids. *Phys. Rev.* **81** 066308. (doi:10.1103/PhysRevE.81.066308).

Karapantsios, T. D. & Karabelas, A. J. 1995 Longitudinal characteristics of wavy falling films. *Int. J. Multiphase Flow* **21**, 119–127. (doi:10.1016/0301-9322(94)00048-O)

Karapantsios, T. D., Paras, S. V. & Karabelas, A. J. 1989 Statistical characteristics of free falling films at high Reynolds numbers. *Int. J. Multiphase Flow* **15**, 1–21. (doi:10.1016/0301-9322(89)90082-7)

Lel, V. V., Al-Sibai, F., Leefken, A. & Renz, R. 2005 Local thickness and wave velocity measurement of wavy films with a chromatic confocal imaging method and a fluorescence intensity technique. *Exp. Fluids*, **39**, 856–864. (doi:10.1007/s00348-005-0020-x)

Llewellin, E. W., Mader, H. M. & Wilson, S. D. R. 2002 The rheology of a bubbly liquid. *Proc. R. Soc. Lond. A* **458**, 987–1016. (doi:10.1098/rspa.2001.0924)

Nicklin, D. J., Wilkes, J. O. & Davidson, J. F. 1962 Two-phase flow in vertical tubes. *Trans. Inst. Chem. Engrs* **40**, 61–68.

Niranjan, K., Hashim, M. A., Pandit, A. B. & Davidson, J. F. 1988 Liquid-phase controlled mass-transfer from a gas slug. *Chem. Eng. Sci.* **43**, 1247–1252. (doi:10.1016/0009-2509(88)85096-6)

Nogueira, S., Riethmuler, M. L., Campos, J. B. L. M. & Pinto, A. M. F. R. 2006 Flow in the nose region and annular film around a Taylor bubble rising through vertical columns of stagnant and flowing Newtonian liquids. *Chem. Eng. Sci.* **61**, 845–857. (doi:10.1016/j.ces.2005.07.038)

Nusseldt, W. 1916 Die Oberflachenkondensation des Wasserdamphes. *Zeitschrift des vereines Deutschem Ingenieure* **60**, 541–546.

Sena Esteves, M. T. & Guedes de Carvalho, J. R. F. 1993 Liquid-side mass-transfer coefficient for gas slugs rising in liquids. *Chem. Eng. Sci.* **48**, 3497–3506. (doi:10.1016/0009-2509(93)85005-A)

Seyfried, R. & Freundt, A. 2000 Experiments on conduit flow and eruption behavior of basaltic volcanic eruptions. *J. Geophys. Res.* **105**, 23 727–23 740. (doi:10.1029/2000JB900096)

Shosho, C. & Ryan, M. 2001 An experimental study of the motion of long bubbles in inclined tubes. *Chem. Eng. Sci.* **56**, 2191–2204. (doi:10.1016/S0009-2509(00)00504-2)

Taha, T. & Cui, Z. F. 2006 CFD modelling of slug flow in vertical tubes. *Chem. Eng. Sci.* **61**, 676–687. (doi:10.1016/j.ces.2005.07.022)

Takahama, H. & Kato, S. 1980 Longitudinal flow characteristics of vertically falling liquid films without concurrent gas flow. *Int. J. Multiphase Flow* **6**, 203–215. (doi:10.1016/0301-9322(80)90011-7)

Vergniolle, S. & Brandeis, G. 1996 Strombolian explosions. I. A large bubble breaking at the surface of a lava column as a source of sound. *J. Geophys. Res.* **101**, 20 433–20 447. (doi:10.1029/96JB01178)

Viana, F., Pardo, R., Yanez, R., Trallero, J. & Joseph, D. 2003 Universal correlation for the rise velocity of long gas bubbles in round pipes. *J. Fluid Mech.* **494**, 379–398. (doi:10.1017/S0022112003006165)

Wallis, G. B. 1969 *One-dimensional two-phase flow*. New York, NY: McGraw-Hill.

White, E. T. & Beardmore, R. H. 1962 The velocity of rise of single cylindrical air bubbles through liquids contained in vertical tubes. *Chem. Eng. Sci.* **17**, 351–361. (doi:10.1016/0009-2509(62)80036-0)

Zheng, D., He, X. & Che, D. 2007 CFD simulations of hydrodynamic characteristics in a gas-liquid vertical upward slug flow. *Int. J. Heat Mass Transfer* **50**, 4151–4165. (doi:10.1016/j.ijheatmasstransfer.2007.02.041)

Zhou, D. W., Gambaryan-Roisman, T. & Stephan, P. 2009 Measurement of water falling film thickness to flat plate using confocal chromatic sensoring technique. *Exp. Thermal Fluid Sci.* **33**, 273–283. (doi:10.1016/j.expthermflusci.2008.09.003)